Inorganic Chemistry

Article

pubs.acs.org/IC

Soluble Sugar-Based Quinoline Derivatives as New Antioxidant Modulators of Metal-Induced Amyloid Aggregation

Valentina Oliveri,[†] Giuseppa I. Grasso,[‡] Francesco Bellia,[‡] Francesco Attanasio,[‡] Maurizio Viale,[§] and Graziella Vecchio*[,†]

[†]Dipartimento di Scienze Chimiche, Università degli Studi di Catania, Viale A. Doria 6, 95125 Catania, Italy

[‡]Istituto di Biostrutture e Bioimmagini (IBB), CNR, Via P. Gaifami 18, 95126, Catania, Italy

[§]IRCCS Azienda Ospedaliera Universitaria San Martino − IST Istituto Nazionale per la Ricerca sul Cancro, U.O.C. Bioterapie, L.go R. Benzi, 10, 16132 Genova, Italy

Supporting Information

ABSTRACT: Oxidative stress and protein aggregation have been demonstrated to be the major factors involved in neurodegenerative diseases. Metal ions play a pivotal role, acting as mediators of neurotoxicity either by favoring or redox cycling. Thus, they represent a promising and suitable therapeutic target for the treatment of neurodegenerative disorders. In particular, the development of bifunctional or multifunctional molecules, which have antiaggregant and metal-chelating/antioxidant properties, may be considered as a valuable strategy for the treatment of neurodegeneration considering its multifactorial nature. Herein, we report the design and the characterization of four new multifunctional sugar-appended 8-hydroxyquinolines focusing on the effects of the conjugation with trehalose, a nonreducing disaccharide involved in the protection of proteins and cells against environmental stresses. These glycoconjugates do not exhibit any antiproliferative activity against three human cell lines of different histological origin, unlike 8-hydroxyquinolines. The multiple properties of the new derivatives are highlighted, reporting their Cu^{2+} and Zn^{2+} binding ability, and antioxidant and antiaggregant capacities. In particular, these latter were determined by different assays, including the evaluation of their ability to modulate or even suppress the aggregation of $A\beta_{1\text{-}40}$ and $A\beta_{1\text{-}42}$ peptides induced by copper or zinc ions.

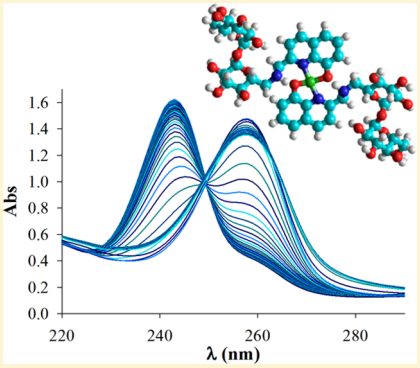

INTRODUCTION

The neurodegenerative diseases are multifactorial in their etiopathology. For this reason, multitarget-directed molecules have recently been proposed as agents more adequate for addressing the complexity of disorders such as Alzheimer's (AD), Parkinson's (PD), Huntington's (HD), and Wilson's (WD) diseases.[1]

Oxidative stress, metal dyshomeostasis, protein misfolding and aggregation are some pathogenic pathways involved in neurodegenerative disorders. In particular, accumulated evidence has revealed that metal ions could be responsible for damage involving oxidative stress, protein modification and aggregation.[2,3] In this context, bi- or multifunctional metal chelators may provide greater efficacy, and better utility as potential drugs. Furthermore, the development of metal-protein attenuating compounds (MPAC) is a promising therapeutic approach for neurodegenerative diseases.[4] Among them, clioquinol (CQ) and PBT2, two 8-hydroxyquinoline (OHQ) derivatives, are reported to have the highest interest in the treatment of AD and HD.[5] Despite its failure as a drug,[6] CQ proved that metal chelation has a good potential for the AD treatment, and the positive outcomes from *in vitro* and clinical studies have inspired other researchers to modify it. The OHQ scaffold has been functionalized in a number of ways by linking it to neuropeptides, masking the chelation site with boronic ester or sugar, or adding acetylcholinesterase and/or monoamine oxidase inhibitor functional groups.[4] However, PBT2 is the best-developed structure for metal chelation toward AD treatment. The mechanism of action has been investigated, and experimental evidence suggests that PBT2 could remove copper and other metals from extracellular amyloid. PBT2 encounters the extracellular pool of metals that are in a dissociable equilibrium with Aβ, binds the metals, and facilitates plaque dissolution. The metal ions may be in a ternary complex with the drug itself or in a complex with Aβ. These complexes are taken up by neighboring cells, where the metal and ligands are separated.[7] Nevertheless, PBT2, as announced by Prana Biotechnology in 2014, did not meet its primary end point of a statistically significant reduction in the levels of beta-amyloid plaques in the brains of prodromal/mild Alzheimer's disease patients.[8]

More recently, bis(8-aminoquinoline) tetradentate ligands, such as PA1637, have been proposed as new drug candidates

Received: November 13, 2014
Published: March 2, 2015

DOI: 10.1021/ic502713f
Inorg. Chem. 2015, 54, 2591−2602

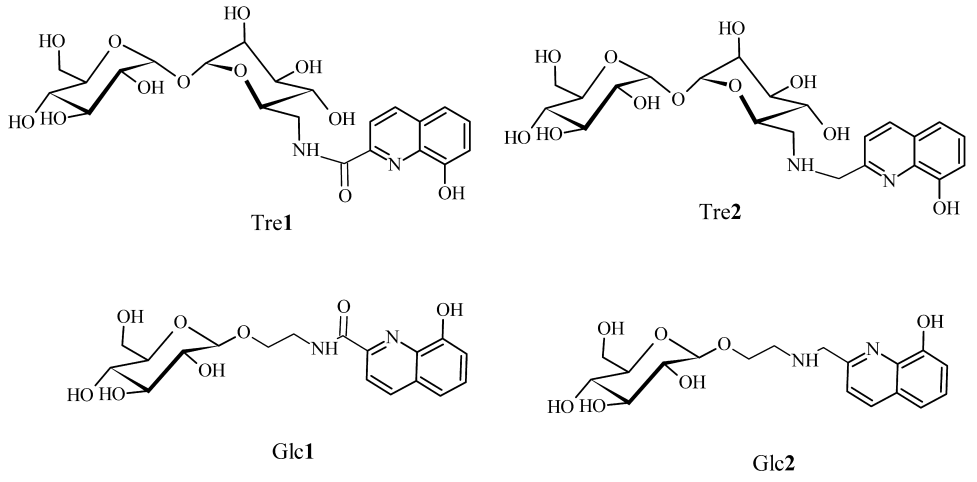

Figure 1. Trehalose (Tre**1**, Tre**2**) and glucose (Glc**1**, Glc**2**) derivatives of 8-hydroxyquinoline (LH).

for the treatment of AD because it has been demonstrated that PA1637 fully reverses the deficit of episodic memory of a nontransgenic mouse AD model, outperforming CQ.[9,10]

We demonstrated in our early investigations that the conjugation of OHQs with sugars ameliorated their properties. Glycoconjugates and their metal complexes are more soluble in water than OHQs,[11−13] and they can be selectively activated by glycosidase enzymes in tumor cells.[14−16] Herein, we report on the investigation of four new glycoconjugates focusing on the effects of the conjugation with trehalose (Tre, α-D-glucopyranosyl α-D-glucopyranoside), a nonreducing sugar. This disaccharide has been known to impart stability to organisms tolerating anhydrobiosis and cryobiosis by protecting proteins and cells against environmental stresses.[17] As an application of its natural capacity to protect biological structures, Tre has been used for the preservation of biological materials during dehydration.[18,19] Furthermore, Tre protects cells from oxidative damage and prevents protein aggregation in yeast.[20] Biological properties of Tre suggest a host of potential uses in neurodegenerative diseases involving protein misfolding and aggregation. In fact, Tre has been reported to interfere with amyloid fibril formation and reduce the cytotoxicity increasing human neuroblastoma cell viability in the presence of Aβ aggregates.[21] Tre is also effective in inhibiting polyglutamine-mediated protein aggregation and alleviating the symptoms in models of HD.[22] Other studies revealed that Tre inhibits fibrillation of alpha-synuclein and disaggregates existing fibrils.[23−25]

In this context, considerable effort has been placed on the synthesis of Tre derivatives with improved properties,[26,27] including the blood brain barrier penetration ability.[28]

In this work, the Tre scaffold is augmented with new functionalities conferred by OHQ. We present the synthesis and characterization of two new Tre compounds and their glucose analogues (Figure 1); we investigated the metal-binding properties of the derivatives with copper and zinc ions.

Moreover, we also evaluated the antiproliferative activity against three human cancer cell lines (A2780, A549, and SHSY5Y) of different histological origin in order to compare these new systems with the OHQ glucosides that we have previously studied.[14,15] Also, we found encouraging results from *in vitro* studies regarding antioxidant and antiaggregant activities. In particular, we tested the ability of these glycoconjugates to inhibit metal-induced aggregation of the model fibril-forming protein, β-lactoglobulin A (BLG), exploiting an assay previously developed by us.[12] Furthermore, since the aggregation of Aβ is a characteristic pathological feature in AD, we also investigated the effect of the new OHQ glycoconjugates on Aβ aggregation induced by Cu^{2+} or Zn^{2+} ions.

EXPERIMENTAL SECTION

Materials. Reagents were purchased from common commercial suppliers and were used without further purification. 6-Amino-6-deoxy-α,α'-trehalose was obtained as reported elsewhere.[29]

4-(2-Hydroxy-ethyl)-1-piperazineethanesulfonic acid (HEPES) buffer (20 mM) was treated with Chelex to remove any residual transition metal ion.

Chromatographic separations were performed on silica gel or CM-sephadex C-25 (NH_4^+ form) columns. Thin layer chromatography (TLC) was carried out on silica gel plates (Merck 60-F254). Compounds were detected on TLC through UV light (λ = 254 nm) and the anisaldehyde test.

Stock solutions of Cu^{2+} and Zn^{2+} salts (nitrate or perchlorate) were prepared by dissolving the corresponding salt in water and titrating the resulting solutions with standardized EDTA using murexide and eriochrome black T, respectively.[30]

Synthesis of 6-Deoxy-6-[(8-hydroxyquinoline)-2-carboxyl]-amino]-α,α'-trehalose (Tre1). 1,3-Dicyclohexylcarbodiimide (DCC, 30 mg, 0.15 mmol) was added to a stirred solution of 1-hydroxybenzotriazole hydrate (HOBt, 23 mg, 0.15 mmol) and 8-hydroxyquinoline-2-carboxylic acid (28 mg, 0.15 mmol) in DMF. After 1 h, 6-amino-6-deoxy-α,α'-trehalose (50 mg, 0.15 mmol) was added, and the mixture was stirred at room temperature for a further 24 h. The solvent was then removed *in vacuo*, and the remaining residue gave, after purification by column chromatography on reverse phase RP-8 (linear gradient $H_2O \rightarrow$ EtOH), the desired product.

Yield: 55%. TLC: R_f = 0.41 (PrOH/AcOEt/H_2O/NH_3 4:3:2:1). Positive ion ESI-MS: m/z = 513.0 $[LH + H]^+$, 535.1 $[LH + Na]^+$. ^{1}H NMR (500 MHz, D_2O, pD = 6.0) δ (ppm): 8.18 (s, 1H, H-4), 7.84 (s, 1H, H-3), 7.40 (m, 1H, H-6), 7.30, (s, 1H, H-5), 7.05 (s, 1H, H-7), 5.08 (s, 1H, H-1A of Tre), 5.01 (s, 1H, H-1B of Tre), 3.90 (s, 1H, H-5A of Tre), 3.83−3.64 (m, 5H, Hs-3, H-5B, H-6A and H-6B of Tre), 3.64−3.53 (m, 3H, H-6′A, H-2A, H-6′B of Tre), 3.34 (m, 2H, H-4A and H-2B of Tre), 3.24 (m, 1H, H-4B of Tre).

^{13}C NMR (125 MHz, D_2O, pD = 6.0) δ (ppm): 165.9 (C═O), 152.4 (C-10), 146.5 (C-2), 138.1 (C-4), 136.4 (C-9), 129.2 (C-6), 118.8 (C-5), 118.4 (C-3), 111.8 (C-7), 93.1(C-1A and C-1B of Tre), 73.6−68.2 (Cs of Tre) 60.2 (C-6B of Tre), 39.9 (C-6A of Tre).

Synthesis of 6-Deoxy-6-(8-hydroxyquinoline)-2-methyl-amino]-α,α'-trehalose (Tre2). 8-Hydroxy-2-quinolinecarboxaldehyde (13 mg, 0.075 mmol) was added to 6-amino-6-deoxy-α,α'-

DOI: 10.1021/ic502713f
Inorg. Chem. 2015, 54, 2591−2602

trehalose (25 mg, 0.074 mmol) in anhydrous methanol (8 mL). After 7 h, sodium triacetoxyborohydride (31 mg, 0.15 mmol) was added. The reaction was refluxed overnight, and then the solvent was evaporated *in vacuo*. The crude product was purified by ion-exchange chromatography on Sephadex CM-25 (linear gradient of NH_4HCO_3 0 → 0.25 M).

Yield: 83%. TLC: R_f = 0.54 (PrOH/AcOEt/H_2O/NH_3 4:3:2:1). Positive ion ESI-MS: m/z = 499.1 [LH + H]$^+$, 521.1 [LH + Na]$^+$, 996.6 [2LH + H]$^+$, 1018.7 [2LH + Na]$^+$. ^{1}H NMR (500 MHz, D_2O, pD = 9.5) δ (ppm): 8.17 (d, 1H, $J_{4,3}$ = 8.4 Hz, H-4), 7.37 (m, 2H, H-3 and H-6), 7.24 (d, 1H, $J_{5,6}$ = 7.8 Hz, H-5), 6.98 (d, 1H, $J_{7,6}$ = 7.4 Hz, H-7), 5.11 (m, 2H, Hs-1 of Tre), 4.04 (m, 2H, CH_2Ar), 3.89 (m, 1H, H-5A of Tre), 3.74 (m, 4H, Hs-3, H-5B, H-6B of Tre), 3.66 (dd, 1H, $J_{6'B,6B}$ = 11.9 Hz and $J_{6'B,5}$ = 4.9 Hz, H-6′B of Tre), 3.55 (dd, 1H, $J_{2A,3A}$ = 9.9 Hz and $J_{2A,1A}$ = 3.0 Hz, H-2A of Tre), 3.51 (dd, 1H, $J_{2B,3B}$ = 9.9 Hz and $J_{2B,1B}$ = 3.5 Hz, H-2B of Tre), 3.34 (t, 1H, J = 9.4 Hz, H-4B of Tre), 3.22 (m, 1H, H-4A of Tre), 2.98 (d, 1H, $J_{6A,6'A}$ = 12.5 Hz, H-6A of Tre), 2.76 (m, 1H, H-6′A of Tre). ^{13}C NMR (125 MHz, D_2O, pD = 9.5) δ (ppm): 156.2 (C-2), 155.6 (C-8), 139.1 (C-9), 137.4 (C-4), 128.8 (C-10), 127.5 (C-6), 120.7 (C-3), 116.1 (C-5), 112.6 (C-7), 93.2 (C-1A and C-1B of Tre), 73.1−71.4 (Cs-3, C-4A, C-5B of Tre), 71.0 (Cs-2 of Tre), 70.3 (C-5A of Tre), 69.6 (C-4B of Tre), 60.5 (C-6B of Tre), 53.4 (CH_2Ar), 49.0 (C-6A of Tre).

Synthesis of 2-(Fmoc-amino)ethyl-2,3,4,6-tetra-*O*-acetyl-*β*-D-glucopyranoside. Boron trifluoride diethyl etherate (1.8 mL) was added dropwise to a solution of *β*-D-glucose pentaacetate (1.67 g, 4.3 mmol) and 9-fluorenylmethyl-*N*-(2-hydroxyethyl)carbamate (1.3 g, 4.6 mmol) in 20 mL of CH_2Cl_2 at 0 °C. After a few minutes, the mixture was heated at room temperature and stirred for 48 h. The reaction was then quenched with water and extracted with CH_2Cl_2. The CH_2Cl_2 layer was collected, dried with Na_2SO_4, and concentrated *in vacuo*. The crude product was purified by silica gel chromatography using ethyl acetate/hexane 3:2 as the eluent.

Yield: 74%. TLC: R_f = 0.42 (AcOEt/Hex 3:2). Positive ion ESI-MS: m/z = 613.9 [P + H]$^+$, 636.1 [P + Na]$^+$, 651.9 [P + K]$^+$. ^{1}H NMR (500 MHz, $CDCl_3$) δ (ppm): 7.79 (t, 2H, $J_{4,3}$ = $J_{5,6}$ = 6.7 Hz, H-4 and H-5 of Fmoc), 7.61 (t, 2H, $J_{1,2}$ = $J_{8,7}$ = 6.5 Hz, H-1 and H-8 of Fmoc), 7.43 (m, 2H, H-3 and H-6 of Fmoc), 7.34 (m, 2H, H-2 and H-7 of Fmoc), 5.22 (t, 1H, J = 9.6 Hz, H-3 of Glc), 5.05 (t, 1H, J = 9.7 Hz, H-4 of Glc), 4.98 (m, 1H, H-2 of Glc), 4.56 (m, 1H, H-9 of Fmoc), 4.49 (m, 1H, CH_2 of Fmoc), 4.36 (d, 1H, $J_{1,2}$ = 7.9 Hz, H-1 of Glc), 4.31−4.03 (m, 3H, CH_2 of Fmoc and Hs-6), 3.79 (m, 1H, OCH_2 of en), 3.71 (m, 1H, OCH_2 of en), 3.59 (m,1H, H-5 of Glc), 3.38 (m, 2H, CH_2N of en), 2.11−2.00 (m, 12H, CH_3).

Synthesis of 2-Aminoethyl-*β*-D-glucopyranoside (GlcN). 2-(Fmoc-amino)-ethyl-2,3,4,6-tetra-*O*-acetyl-*β*-D-glucopyranoside (1.0 g, 1.63 mmol) was stirred in methanol (25 mL) with sodium methoxide (CH_3OH solution, 2.4 mL, 0.5 M) at room temperature overnight. The reaction mixture was concentrated *in vacuo*. The resulting residue was dissolved in water, and the aqueous solution was extracted with CH_2Cl_2. The aqueous layer was lyophilized, and the product, GlcN, was used without further purification.

Yield: 85%. ESI-MS: m/z = 224.0 [P + H]$^+$, 246.0 [P + Na]$^+$, 446.7 [2P + H]$^+$, 468.7 [2P + Na]$^+$. ^{1}H NMR (500 MHz, CD_3OD) δ (ppm): 4.39 (d, 1H, $J_{1,2}$ = 8.0 Hz, H-1), 3.91 (m, 1H, CH_2O) 3.82 (m, 1H, H-6), 3.70 (m, 1H, CH_2O), 3.62 (m, 1H, H-6′), 3.38 (m, 2H, H-3 and H-5), 3.29 (m, 1H, H-4), 3.21 (m, 1H, H-2), 2.89 (s, 2H, CH_2N). ^{13}C NMR (125 MHz, D_2O) δ (ppm): 102.3 (C-1), 75.6 (C-3 and C-5), 73.0 (C-2), 69.5 (CH_2O, C-4), 60.5 (C-6), 39.7 (CH_2N).

Synthesis of 2-[(8-Hydroxyquinoline)-2-carboxyl]amino-ethyl]-*β*-D-glucopyranoside (Glc1). HOBt (91 mg, 0.67 mmol) and DCC (138 mg, 0.67 mmol) were added to a suspension of 8-hydroxyquinoline-2-carboxylic acid (127 mg, 0.67 mmol) in dry DMF (10 mL). After 0.5 h, GlcN (150 mg, 0.67 mmol) was added. The reaction mixture was stirred for 48 h at room temperature. The solvent was then removed *in vacuo*, and the remaining residue gave, after purification by column chromatography on reverse phase RP-8 (linear gradient H_2O → CH_3OH), the desired product.

Yield: 68%. TLC: R_f = 0.70 (CH_3OH). Positive ion ESI-MS (CH_3OH): m/z = 394.9 [LH + H]$^+$, 417.1 [LH + Na]$^+$, 433.1 [LH + K]$^+$, 810.7 [2LH + Na]$^+$, 827.1 [2LH + K]$^+$. Negative ion ESI-MS (CH_3OH): m/z = 393.1 [L]$^-$, 808.9 [2LH − 2H + Na]$^-$. ^{1}H NMR (500 MHz, CD_3OD) δ (ppm): 8.41 (d, 1H, $J_{4,3}$ = 8.6 Hz, H-4), 8.19 (d, 1H, $J_{3,4}$ = 8.6 Hz, H-3), 7.54 (t, 1H, J = 7.9 Hz, H-6), 7.41 (d, 1H, $J_{5,6}$ = 7.7 Hz, H-5), 7.16 (d, 1H, $J_{7,6}$ = 7.5 Hz, H-7), 4.37 (d, 1H, $J_{1,2}$ = 7.8 Hz, H-1 of Glc), 4.13 (m, 1H, CH_2), 3.84 (m, 3H, CH_2, H-5 of Glc), 3.69 (m, 2H, CH_2, H-4 of Glc), 3.40−3.17 (m, 4H, H-3, Hs-6, H-2 of Glc). ^{13}C NMR (125 MHz, D_2O) δ (ppm): 165.5 (C═O), 153.7 (C-2), 147.3 (C-8), 137.4 (C-4), 137.0 (C-9), 130.1 (C-10), 129.2 (C-6), 118.6 (C-5), 117.5 (C-3), 111.4 (C-7), 103.2 (C-1 of Glc), 76.6 (C-3 and C-5 of Glc), 73.7 (C-2 of Glc), 70.1 (C-4 of Glc), 68.2 (−OCH_2), 61.3 (C-6 of Glc), 39.5 (CH_2N−).

Synthesis of 2-[(8-Hydroxyquinoline)-2-methylaminoethyl]-*β*-D-glucopyranoside (Glc2). 8-Hydroxy-2-quinolinecarboxaldehyde (19 mg, 0.11 mmol) was added to GlcN solution (25 mg, 0.11 mmol) in anhydrous methanol (8 mL). After 7 h, sodium triacetoxyborohydride (45 mg, 0.22 mmol) was added. The reaction was refluxed overnight, and then the solvent was evaporated *in vacuo*. The crude product was purified by ion-exchange chromatography (Sephadex CM-25, linear gradient of NH_4HCO_3 0 → 0.25 M).

Yield: 70%. TLC: R_f = 0.57 (PrOH: AcOEt: H_2O: NH_3 4:3:2:1). Positive ion ESI-MS: m/z = 381.2 [LH + H]$^+$, 403.1 [LH + Na]$^+$. Negative ion ESI-MS: m/z = 379.1 [L]$^-$. ^{1}H NMR (500 MHz, D_2O) δ (ppm): 8.23 (d, 1H, $J_{4,3}$ = 8.5 Hz, H-4), 7.48−7.32 (m, 3H, H-3, H-5 and H-6), 7.09 (d, 1H, $J_{7,6}$ = 7.3 Hz, H-7), 4.88 (d, 1H, $J_{1,2}$ =7.9 Hz, H-1 of Glc), 4.18 (m, 2H, CH_2Ar), 4.02 (m, 1H, −OCH_2), 3.83 (m, 1H, −OCH_2), 3.76 (m, 1H, H-6 of Glc), 3.54 (dd, 1H, $J_{6',6}$ = 12.3 Hz, $J_{6',5}$ = 6.0 Hz, H-6′ of Glc), 3.36 (m, 2H, H-3 and H-5 of Glc), 3.24 (m, 2H, H-2 and H-4 of Glc), 3.01 (m, 2H, CH_2N−). ^{13}C NMR (125 MHz, D_2O) δ (ppm): 155.1 (C-2), 153.1 (C-8), 138.2 (C-9), 137.6 (C-4), 128.3 (C-10), 127.4 (C-6), 120.7 (C-3), 117.7 (C-5), 112.0 (C-7), 102.1 (C-1 of Glc), 76.3−74.8 (C-3 and C-5 of Glc), 73.1 (C-2 of Glc), 69.4 (C-4 of Glc), 67.5 (−OCH_2), 60.5 (C-6 of Glc), 52.7 (CH_2Ar), 47.7 (CH_2N−).

NMR Spectroscopy. ^{1}H and ^{13}C NMR spectra were recorded at 25 °C with a Varian UNITY PLUS-500 spectrometer at 499.9 and 125.7 MHz, respectively. The NMR spectra were obtained by using standard pulse programs from the Varian library. The 2D experiments (COSY, TOCSY, gHSQCAD, gHMBC) were acquired using 1K data points, 256 increments, and a relaxation delay of 1.2 s. The spectra were referred to the solvent signal. A and B refer to the functionalized and the unfunctionalized glucose rings of Tre.

Circular Dichroism Spectroscopy. Circular dichroism measurements were performed with a JASCO J-1500 spectropolarimeter. The spectra represent the average of 5 scans and were recorded at 25 °C, on freshly prepared solutions.

Potentiometric Measurements. Potentiometric titrations were performed by means of two home-assembled, fully automated apparatus sets (Metrohm E654 pH-meter, Metrohm combined pH glass electrode 6.0234.100, Hamilton Microlab 500 series dispenser) controlled by the appropriate software set up in our laboratory. The titration cell (2 mL) was thermostated at 25.0 ± 0.2 °C, and all solutions were kept under an atmosphere of argon. The system was calibrated on the pH = −log [H$^+$] scale by titrating HNO_3 with CO_2-free base. The values of $E°$, E_j, K_w, and the Nernstian slope of the electrode system were determined in separate experiments by titrating nitric acid with CO_2-free potassium hydroxide. Base solutions (0.1 M) were added through a Hamilton buret equipped with a 1 mL syringe. In order to determine the protonation constants of Tre**1** and Tre**2**, solutions of the ligands with concentrations ranging from 2.0 to 3.0 mM were titrated with 0.1 M potassium hydroxide. Three independent runs were collected, each run including 50−60 points. The initial pH was always adjusted to 2.1. To avoid systematic errors and verify the reproducibility, the emf values of each experiment were taken at different time intervals. The ionic strength was maintained at 0.1 M (KNO_3). Other experimental details have been reported previously.[31]

Spectrophotometric Measurements. UV−vis titrations were carried out with an Agilent 8453 diode-array spectrophotometer interfaced with a home-assembled potentiometric apparatus (Metrohm E654 pH-meter, Orion 9103SC combined micro pH glass electrode,

DOI: 10.1021/ic502713f
Inorg. Chem. 2015, 54, 2591−2602

Hamilton Microlab 500 series dispenser), all controlled by a software set up in our laboratory. The quartz cell (1 cm path length) was thermostated at 25.0 ± 0.2 °C. In order to double check the proton complexes constant values and to determine the stability constants for the Cu^{2+} and Zn^{2+} complexes, solutions of the ligands (from 4.0 to 5.0 × 10^{-5} M) or the ligands (from 4.0 to 5.0 × 10^{-5} M) and the metals (M/L ratios ranged from 0.5 to 2) were titrated with potassium hydroxide solutions (0.05015 M). Base solutions were added through a Hamilton buret equipped with a 1 mL syringe. The ionic strength of all solutions was adjusted to 0.1 M ($NaClO_4$). Six independent titrations were carried out, each including 60−70 points. The initial pH was adjusted to 2.4 for all solutions.

Calculations. $E°$ and K_w values were determined by the computer program ACBA.[32] Potentiometric and spectrophotometric data were handled with the software Hyperquad,[33] which carries out a nonlinear minimization of the sum of the squared residuals U and also allows for the simultaneous refinement of data from different titrations

$$U = \sum (E_{exp} - E_{calc})^2$$

where E_{exp} and E_{calc} are the experimental and the calculated electrode potentials, respectively. The species distribution was calculated by using the program Hyss.[34]

Mass Spectrometry. ESI-MS measurements were carried out by using a Finnigan LCQ DECA XP PLUS ion trap spectrometer operating in the positive or negative ion mode and equipped with an orthogonal ESI source (Thermo Electron Corporation, USA). Cu^{2+} and Zn^{2+} complexes for ESI-MS studies were prepared by adding a solution of $CuSO_4$ or $ZnSO_4$ to a ligand solution. Different metal ligand ratios were investigated. Sample solutions were injected into the ion source without the addition of any other solvent at a flow rate of 5 μL/min. For electrospray ionization, the drying gas (nitrogen) was heated at 260 °C. The capillary exit and skimmer voltage were varied in order to optimize the signal responses. Scanning was performed from m/z = 100 to 2000. Xcalibur software was used for the elaboration of mass spectra. The assignments of the peaks in ESI-MS spectra were done by comparing the experimental isotopic patterns with the corresponding simulated profiles. Each species is indicated with the m/z value of the first peak of its isotopic cluster.

Antiproliferative Activity. All glycoconjugates were dissolved in dimethyl sulfoxide (DMSO) at the concentration of 100 mM and then diluted in fetal calf serum (FCS, final DMSO concentration on cells 0.2−1%).

Human cell lines A2780 (ovary, adenocarcinoma), A549 (lung, carcinoma) cultured in RPMI 1640 medium (plus antibiotics, L-glutamine, and 10% fetal calf serum), and SHSY5Y (neuroblastoma, cultured in MEM medium plus Ham's F12 medium (1:1) plus antibiotics, L-glutamine and 10% fetal calf serum) were plated at appropriate concentrations in 180 μL into flat-bottomed 96-well microtiter plates. After 6−8 h, they were treated with the compounds diluted in FCS in the presence or absence of Cu^{2+} (20 μM $CuCl_2$). After 72 h, the plates were processed and IC_{50}s values were calculated on the basis of the analysis of single concentration−response curves. Each experiment was repeated 4−10 times.

Trolox Equivalent Antioxidant Capacity Assay. The antioxidant capacity of the tested compounds was determined by 2,2′-azinobis(3-ethylbenzothiazoline-6-sulfonic acid) diammonium salt (ABTS) radical cation decolorization assay using 6-hydroxy-2,5,7,8-tetramethylchroman-2-carboxylic acid (Trolox) as a standard. Briefly, the radical cation $ABTS^{+•}$ was generated by a reaction between ABTS (7.00 mM) and persulfate (2.45 mM) in water. After a 16 h incubation (dark, room temperature), the resulting solution was diluted in the cuvette with phosphate buffer (5 mM, pH 7.4) such that the absorbance of the solution at 734 nm was 0.70 ± 0.02. This radical solution was combined with antioxidant samples, in varying concentrations, and allowed to react for 6 min. All samples were diluted to provide 20−80% inhibition of the blank absorbance. The absorbance values were measured for 6 min. Solution absorbance was plotted vs compound concentration; each resultant slope was normalized with respect to that obtained for Trolox to give the Trolox-equivalence (TEAC) value for each time point (1, 3, 6 min). All determinations were carried out at least three times and in triplicate at each separate concentration of the samples in order to obtain consistent data with statistical error.

DPPH Assay. 1,1-Diphenyl-2-picryl-hydrazyl ($DPPH^•$) is a stable free radical which has an unpaired valence electron at one atom of nitrogen bridge. The scavenging of this radical is the basis of the assay.

A methanol solution of the radical $DPPH^•$ was prepared and protected from light. Absorbance was recorded to check the stability of the radical throughout the time of analysis.

Absorbance at 515 nm was recorded at different time intervals for 1 h. The initial absorbance of DPPH was close to 1.00 in all cases. The blank reference cuvette contained methanol (80%) and water (20%). All measurements were performed in triplicate. Six different concentrations of each compound studied have been assayed in order to check the linearity of response and to establish the antioxidant activity values in the adequate linear range. All phenolic compounds were properly dissolved in an aqueous or methanol solution.

Reaction kinetics of the tested compounds with $DPPH^•$ were registered for each antioxidant concentration tested. From these plots, the percentage of $DPPH^•$ remaining at 1 h was calculated using the following equation.

$$\%DPPH = \frac{A_{sample}}{A_{control}} \times 100$$

where $A_{control}$ and A_{sample} represent the absorbances at 515 nm of the radical in the absence and presence of antioxidant, respectively.

The EC_{50} value (the concentration which causes the 50% quenching of DPPH radical) of each sample was obtained plotting the % DPPH• remaining of each concentration of compounds versus the concentration.

Dynamic Light-Scattering Measurements. Dynamic light-scattering (DLS) measurements were carried out using a Zetasizer Nano ZS (Malvern Instruments, U.K.) equipped for backscattering at 173° with a 633 nm He−Ne laser. Protein solutions (0.08 mM) were buffered at pH 7.0 (MOPS, 10 mM). Each DLS measurement was run using automated, optimal measurement times and laser attenuation settings. Zinc-mediated aggregation was studied using Zn^{2+} stock solution in order to obtain Zn^{2+}-BLG of 2. Temperature scanning was realized by increasing the temperature of 2 °C with an equilibration time of 5 min. A measurement of 10 runs was carried out for each temperature. As for the measurements carried out in the presence of the glycoconjugates, these latter compounds were added in equimolar amount to metals.

Aβ Preparation. $Aβ_{1-40}$ or $Aβ_{1-42}$ (Bachem) was dissolved in trifluoroacetic acid (TFA) at a concentration of 1 mg/mL and sonicated for 10 min. TFA was removed by gentle streaming of argon. The peptide was then dissolved in 1,1,1,3,3,3-hexa-fluoro-2-propanol (HFIP) and incubated at 37 °C for 1 h. Following argon streaming, $Aβ_{1-40}$ or $Aβ_{1-42}$ was dissolved again in HFIP, lyophilized, and then suspended in anhydrous DMSO up to 200 μM before the final dilution in HEPES buffer for the turbidimetric assay.

Metal-Induced Aβ Aggregation Assay. The amyloid aggregation process was monitored by light-scattering assay, which reports the change in solution turbidity as a result of precipitate formation. Turbidity is assessed as the difference in absorbance at 405 nm between the sample and its matched control that contains the same components except Aβ peptide. Such an absorbance variation is proportional to the formation of the larger Aβ aggregates, including fibrillar and amorphous ones.[35] Therefore, this method provides an important preliminary evaluation of the aggregation propensity of amyloid peptides in the presence of pro- or antiaggregating agents.

The glucose and trehalose derivatives of OHQ were dissolved in HEPES buffer (20 mM) at pH 6.6 or 7.4 for Cu^{2+} or Zn^{2+} assays, respectively. The pH value for Cu^{2+} was chosen as Cu^{2+}-induced aggregation is optimal at pH 6.6.[36] After the addition of $Aβ_{1-40}$ or $Aβ_{1-42}$ (20 μM), previously dissolved in DMSO, the mixtures were loaded with standardized solutions of $Cu(NO_3)_2$ or $Zn(NO_3)_2$. The molar ratio between Aβ, metal ion, and ligand, was 1:1:3. The metal-induced aggregation assay was performed on flat-bottomed 96-well

DOI: 10.1021/ic502713f
Inorg. Chem. 2015, 54, 2591−2602

plates (Nalge-Nunc, Rochester, NY) incubated at 37 °C in the microplate reader Varioskan (Thermo-fisher) programmed to agitate the plate for 30 s before measuring absorbance at 405 nm every 10 min. Positive and negative controls were used to ensure the validity of the results. Turbidity was monitored by the difference in absorbance at 405 nm between the sample and its matched control that did not contain Aβ.

Native Polyacrylamide Gel Electrophoresis (Native PAGE) and Western Blotting. Reaction samples were loaded on 10−20% gradient Tris-tricine minigels (Invitrogen). Proteins were blotted onto nitrocellulose membranes (Amersham-GE Healthcare), blocked with Odyssey blocking buffer (LI-COR Biosciences), and incubated with a solution (1:1000 dilution) of 6E10 anti-Aβ primary antibody (Covance) overnight at 4 °C. Proteins were then visualized after the incubation (1:30000 dilution) with fluorescent secondary antibodies coupled to IR Dye 680 (LI-COR Biosciences). Infrared fluorescence was measured by scanning the plate using an Odyssey Infrared Imaging System (LI-COR Biosciences).

RESULTS AND DISCUSSION

Synthesis and Characterization. OHQ was conjugated with Tre through two different approaches in order to obtain two compounds with potentially different properties.

Tre**1** was synthesized by an amide condensation reaction starting from the 6-amino-6-deoxy-α,α'-trehalose and 8-hydroxyquinoline-2-carboxylic acid in the presence of HOBt and DCC (Figure S1, Supporting Information). The pure product was isolated, and the characterization and unequivocal structural assignments were achieved by a combination of techniques including ESI-MS and NMR that confirmed the identity of the product. In the ESI mass spectrum, the peaks due to the proton and sodium adducts are evident at m/z 513.1 and 535.1, respectively.

The ^{1}H NMR spectrum of Tre**1** displays the signals due to the quinoline ring and trehalose moiety, the former resonating in the aromatic region between 8.18 and 7.05 ppm (Figure S2, Supporting Information). However, the proton resonances of the aromatic moiety are strongly influenced by the sample concentration, suggesting intermolecular interaction. As for trehalose moiety, 2D spectra allowed unambiguous assignment of all protons and carbons (Figures S3−S4, Supporting Information). The H-1A and H-1B resonate at 5.07 and 5.00 ppm upon the functionalization. Furthermore, H-5A is shifted downfield at 3.92 ppm. It is noteworthy that C-6A carbon is significantly shifted at 39.7 ppm compared to C-6B (60.1 ppm), as expected.

Tre**2** was synthesized by a stepwise reductive amination (Figure S5, Supporting Information). In brief, the reaction of the aldehyde with 6-amino-6-deoxy-α,α'-trehalose involved the preformation of the intermediate imine that was reduced by $NaBH(OAc)_3$. The final product was isolated through ion-exchange chromatography and obtained in a good yield. The ESI mass spectrum of Tre**2** in aqueous solution is essentially constituted by the peaks due to singly charged ions at m/z 499.1 and 521.1 attributable to $[LH + H]^+$ and $[LH + Na]^+$ ions and singly charged dimeric proton and sodium ion adducts at m/z 996.6 and 1018.7.

As for NMR characterization, the aromatic protons are evident in the range of 8.17−6.98 ppm (Figures S6−S9, Supporting Information). Hs-1 appear at 5.11 ppm. The diastereotopic Hs-6 of the A ring are detected at 2.98 and 2.76 ppm, and the H-5A signal is shifted downfield at 3.89 ppm. The H-2A and H-2B are overlapped, whereas the H-4B and H-4A resonate at 3.34 and 3.22 ppm, respectively. The diastereotopic protons of the benzylic CH_2 show up at 4.04 ppm.

For comparison, analogous glucose conjugates were also synthesized. Glc**1** and Glc**2** were obtained starting from 2-aminoethyl-β-D-glucopyranoside (Figures S10−S11, Supporting Information). The latter was obtained by Lewis acid mediated glycosylation of glucose pentaacetate with Fmoc-protected aminoethanol.

Positive ion ESI-MS spectra confirmed the identity of the products. ESI-MS spectra of Glc**1** and Glc**2** show a host of peaks due to singly charged ion adducts with proton, sodium and potassium and dimeric sodium and potassium adducts. In the negative mode, the base peak can be assigned to the singly charged $[L]^-$, presumably due to the deprotonation of the phenolic group.

^{1}H NMR spectra display the peaks due to the quinoline moiety, the glucose unit, and the ethylenic chain (Figures S12−S16, Supporting Information). The former show up in the aromatic region δ = 8.5−7.0 ppm.

Anomeric proton of the sugar resonates as a doublet with coupling constants of 7.8−7.9 Hz, confirming the β-configuration at the anomeric center. The other sugar protons and the diastereotopic ethylenic protons appear in the range δ = 4.2−3.0 ppm.

Acid−Base Properties. The protonation constants of Tre**1** and Tre**2** were potentiometrically determined in aqueous solution at 25 °C and ionic strength I = 0.1 M.

The protonation equilibria of Tre**1** and Tre**2** (L^- is the fully deprotonated form of the ligand) in aqueous solution are given in the following equations

$$L^- + H^+ \rightleftarrows LH \quad (L = \text{Tre}\mathbf{1} \text{ or Tre}\mathbf{2}) \tag{1}$$

$$LH + H^+ \rightleftarrows LH_2^+ \quad (L = \text{Tre}\mathbf{1} \text{ or Tre}\mathbf{2}) \tag{2}$$

$$LH_2^+ + H^+ \rightleftarrows LH_3^{2+} \quad (L = \text{Tre}\mathbf{2}) \tag{3}$$

and the protonation constant values are reported in Table 1 along with those of pyridine (Py), 2-(methylaminomethyl)-pyridine (MAMPy), and OHQ[37] reported for comparison.

Table 1. log K Values for the Protonation of Py, MAMPy, OHQ, Tre1, and Tre2 at 25 °C and I = 0.10 M[a]

log K	Py[37]	MAMPy[37]	OHQ[37]	Tre**1**	Tre**2**
log K_1	5.25	9.01	9.65	8.62(6)	10.20(9)
log K_2		1.91	4.97	1.1(3)	8.07(9)
log K_3					1.1(3)

[a] 3σ in parentheses.

The log K values for Tre**1** are related to the protonation of the phenolate and pyridine groups, and those of Tre**2** are due to amino, phenolate, and pyridine groups. As reported for similar systems,[38,39] the functionalization of the quinoline ring causes a variation of OHQ protonation constants. This variation is restrained for phenolate ranging from 9.65 of OHQ to 8.62 of Tre**1** or 8.07 of Tre**2** and more emphasized for pyridine protonation (4.97 vs 1.1). The decrease of the latter value is similar to that reported for other pyridine derivatives such as MAMPy. Also in this case, the protonation constant is lower than that of pyridine (1.91 vs 5.25). The log K values obtained are in keeping with those of analogous systems.[40]

The distribution diagram of protonated species (Figure S17, Supporting Information) shows that Tre**1** mainly exists as a neutral species at pH 7; over pH 10, Tre**1** is totally deprotonated.

DOI: 10.1021/ic502713f
Inorg. Chem. 2015, 54, 2591−2602

Tre**2** exists as a prevalent cationic species, (Tre**2**)H_2 and as a minor zwitterionic form (Tre**2**)H (amino nitrogen protonated and phenolate deprotonated) at physiological pH (Figure S18, Supporting Information).

Furthermore, log *K* values for the protonation were spectrophotometrically confirmed, and the titration data for Tre**1** and Tre**2** (pH 2.4−10.5) are given in Figure 2.

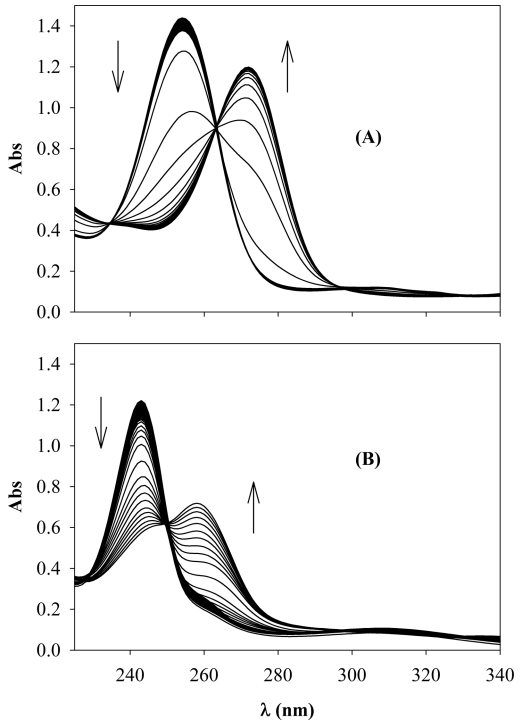

Figure 2. UV−vis titration of Tre**1** (4.2×10^{-5} M) (A) and Tre**2** (4.5×10^{-5} M) (B) with KOH in water at 25 °C and I = 0.1 M ($NaClO_4$).

The electronic spectra of the deprotonated form of Tre**1** and Tre**2** are characterized by a main absorption band centered at 272 and 260 nm, with weak and broad absorption bands at 348 and 412 nm and 342 and 375 nm, respectively. The protonation of the phenolate units leads to the concomitant hypsochromic shift and blending of these two absorption bands to a single one centered at 310 and 316 nm for Tre**1** and Tre**2**, whereas the electronic transitions lying at higher energies are accordingly blue-shifted to 254 and 243 nm, respectively. The UV bands of these compounds could be assigned to the $\pi-\pi^*$ and $n-\pi^*$ transitions, as reported elsewhere.[40]

Metal Complexes. Considering the crucial role of copper and zinc in the etiology of neurodegenerative disorders, Cu^{2+} and Zn^{2+} complexes of the conjugates were characterized by several techniques, such as UV−vis, ESI-MS spectrometry, CD, and NMR spectroscopy.

ESI-MS. A picture of the metal−ligand complexes formed in solution from the new ligands has been obtained by the mass spectrometry data (Figure S19, Supporting Information). The ESI-MS characterization of the Cu^{2+} complexes is reported in Table S1 (Supporting Information). The ESI-MS experiments were carried out at different pHs (5.0−9.0) and various M/L ratios in order to explore the stoichiometry of metal complexes. In addition to the peak of the ligand, new peaks due to the singly charged species $[CuL]^+$ and $[CuL - H + Na]^+$ and singly charged dimeric species appear in the presence of Cu^{2+}. CuL^+ is the main species over the explored pH range (pH 5.0−9.0). ML_2 species are essentially observed for M/L ≤ 0.5. A dinuclear dimeric species is also observed for M/L ≥ 1.

ESI-MS spectra were also recorded in the presence of different amounts of Zn^{2+} at different pHs (Table S2, Supporting Information). The detected species are similar to those of copper; however, the relative intensity of the peaks due to the zinc complexes is much lower than that of copper complexes, suggesting a minor affinity of the ligand for this metal ion, in keeping with the Irving−Williams series.

Finally, it is worth noting that the same species were detected for Tre and Glc derivatives, as expected.

UV−vis Spectroscopy and Potentiometry. Tre**1** and Tre**2** metal complexes were investigated by UV−vis spectroscopy.

As for Cu^{2+}-Tre**1**, the absorption bands of the Tre derivative dramatically change upon addition of the base (Figure S20, Supporting Information). The UV band at 254 nm gradually decreased with concomitant appearance of other bands. In particular, at basic pH, the band at 267 nm with a shoulder at 307 nm and a band at 411 nm were detected. These findings are characteristic of the OHQ derivatives when the complexation is accompanied by the deprotonation of the phenolic group.[11] The shoulder band at 307 nm could be due to a charge-transfer transition $N^- \rightarrow 3d$, involving the deprotonated amide group. As expected, this band is not detected in the Zn^{2+}-Tre1 system (Figure S21, Supporting Information).

Spectrophotometric titrations of Cu^{2+}-Tre**2** solutions (M/L ratios from 0.5 to 2) were characterized at acidic pH by absorption maxima at 243 and 310 nm due to ligand-centered (LC) transitions (Figure 3 and Figure S22, Supporting Information); the intense band that lies in the 225−250 nm region has been attributed to a $\pi-\pi^*$ transition, whereas the less intense and broader band at lower energy is associated with a transition in which substantial charge density is transferred from the oxygen atom to the quinoline moiety.[41] Moving to higher pH values, hypochromic shifts of the LC bands are observed and the appearance of ligand-to-metal charge transfer (LMCT) transitions occur at 258 and 368 nm with corresponding isosbestic points at 248 and 332 nm.

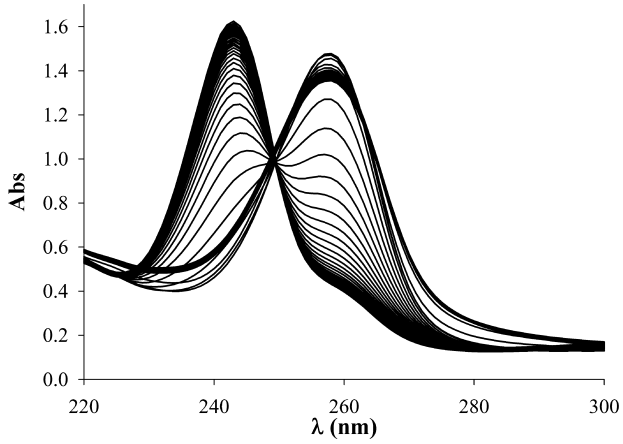

Figure 3. UV−vis titration for Cu^{2+}-Tre**2** system with KOH in water at 25 °C and I = 0.1 M ($NaClO_4$), $C_{Tre2} = 4 \times 10^{-5}$ M.

A similar trend was observed for Zn^{2+}-Tre**2** (Figure S23, Supporting Information).

Furthermore, the stability constants of the Cu^{2+} or Zn^{2+} complexes of Tre**2** were evaluated.

DOI: 10.1021/ic502713f
Inorg. Chem. 2015, 54, 2591−2602

Table 2. Successive Stability Constants for Cu^{2+} and Zn^{2+} Complexes with CQ, OHQ, (DMAM-OHQ), and Tre2

	CQ[38]		OHQ[38]		DMAM-OHQ[40]		Tre2	
	log K_1	log K_2	log K_1	log K_2	log K_1	log K_2	log K_1	log K_2
Cu^{2+}	12.5	10.9	13.5	12.7	14.2	8.3	15.98(1)	10.91(6)
Zn^{2+}	8.5	7.6	9.9	8.9			11.8(2)	8.4(3)

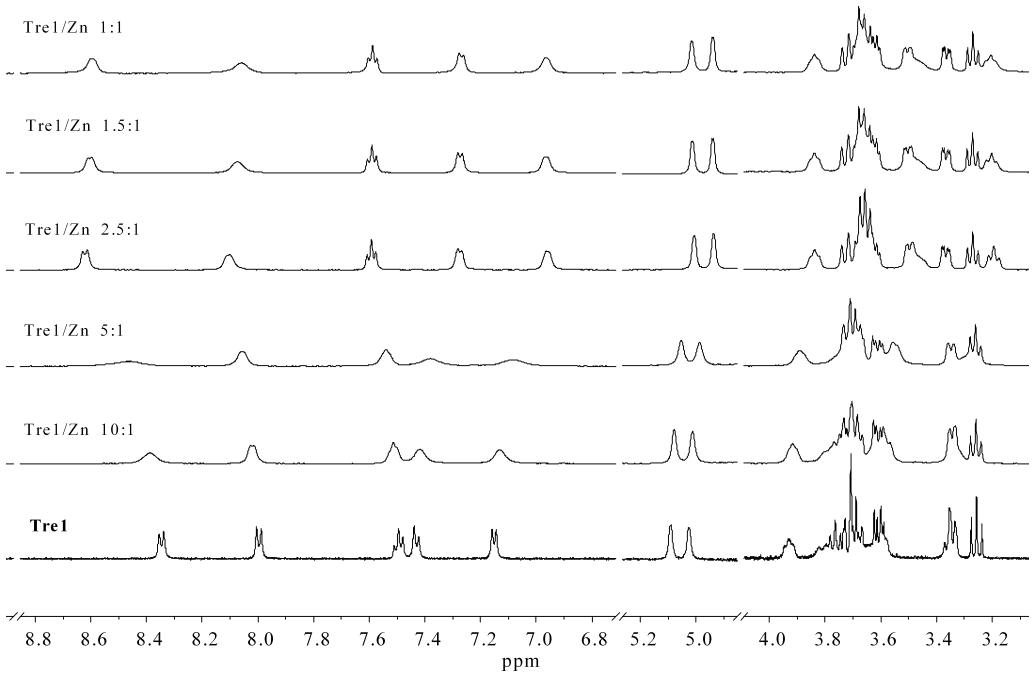

Figure 4. ^1H NMR spectra of Tre**1** with $ZnCl_2$ in D_2O at pD 7.4.

The UV−vis titration data were refined to obtain the best set of complex formation constant values; several models, and combinations thereof were evaluated through the Hyperquad 2006 program. However, the data were satisfactorily fitted by the model reported below:

$$M^{2+} + L^{-} \rightleftarrows [ML]^{+} \quad (M = Cu^{2+} \text{ or } Zn^{2+};\ L = \text{Tre}\mathbf{2}) \tag{4}$$

$$[ML]^{+} + L^{-} \rightleftarrows [ML_2] \tag{5}$$

The stability constant values for the equilibria (eqs 4 and 5) are reported in Table 2.

For comparison, Table 2 also shows the successive stability constant values of CQ,[38] OHQ,[38] and 2-[(dimethylamino)-methyl]-8-hydroxyquinoline (DMAM-OHQ).[40]

From the data reported in Table 2, it is worth noting that the presence of the sugar does not decrease the affinity of the OHQ moiety for metal ions as revealed by K_1 values.

In addition to the donor atoms of the quinoline moiety, another potential donor atom (amino nitrogen) can be identified in Tre**2**. As expected, the stability constant of Tre**2** is significantly higher than that of OHQ because the amino group can coordinate the metal ion stabilizing the complex CuL in comparison with OHQ.

Tre**2** also forms the CuL_2 species, but K_2 values are significantly lower than that of OHQ probably because the presence of an exocyclic donor atom destabilizes the ML_2 species, as in the case of DMAM-OHQ. A similar trend has also been found for the conditional stability constants of cyclodextrin-OHQ conjugates.[11,12]

Zn^{2+} complexes of Tre**2** are less stable than the copper complexes, in keeping with the Irving−Williams series. Also in this case, the K_1 constant value is higher than that of OHQ, supporting the involvement of the amino group in the binding of the zinc ion. A similar behavior has been reported in the case of Zn^{2+} complexes of 2-methylamine-OHQ.[42]

Circular Dichroism. The formation of copper complexes with the glycoconjugates was investigated by CD spectroscopy (Figures S24−S27, Supporting Information). The titration of the ligands with $CuSO_4$ at pH 7.4 dramatically affected their CD spectra.

Intense dichroic bands are present in the CD spectra of the metal complexes. The CD spectra of all the ligands show weak bands because the sugar moiety induces chirality in the region of $\pi-\pi^*$ transitions of the aromatic rings. The intensity of the bands increased when Cu^{2+} is added. The CD bands due to CT transitions appeared in the spectra. In particular, CD spectra of Cu^{2+}-Tre**2** show an intense dichroic signal with a negative band at 256 nm, a positive band at 272 nm, and a small positive band at 227 nm. The Cu^{2+}-Glc**2** and Cu^{2+}-Tre**2** systems have specular spectra. In both cases, the spectra changed until the M/L ratio 1:1 was reached. This behavior is in keeping with the formation of complex ML with the exocyclic nitrogen atom involved in the metal coordination that renders the system more rigid and intensity of CD bands higher. As for Cu^{2+}-Tre**1** when the ratio M/L = 0.5 was reached, the CD spectra showed weak bands. At M/L > 1, the bands became more intense, in keeping with the involvement of an exocyclic nitrogen in the metal binding. A similar behavior was found for Glc**1**.

DOI: 10.1021/ic502713f
Inorg. Chem. 2015, 54, 2591−2602

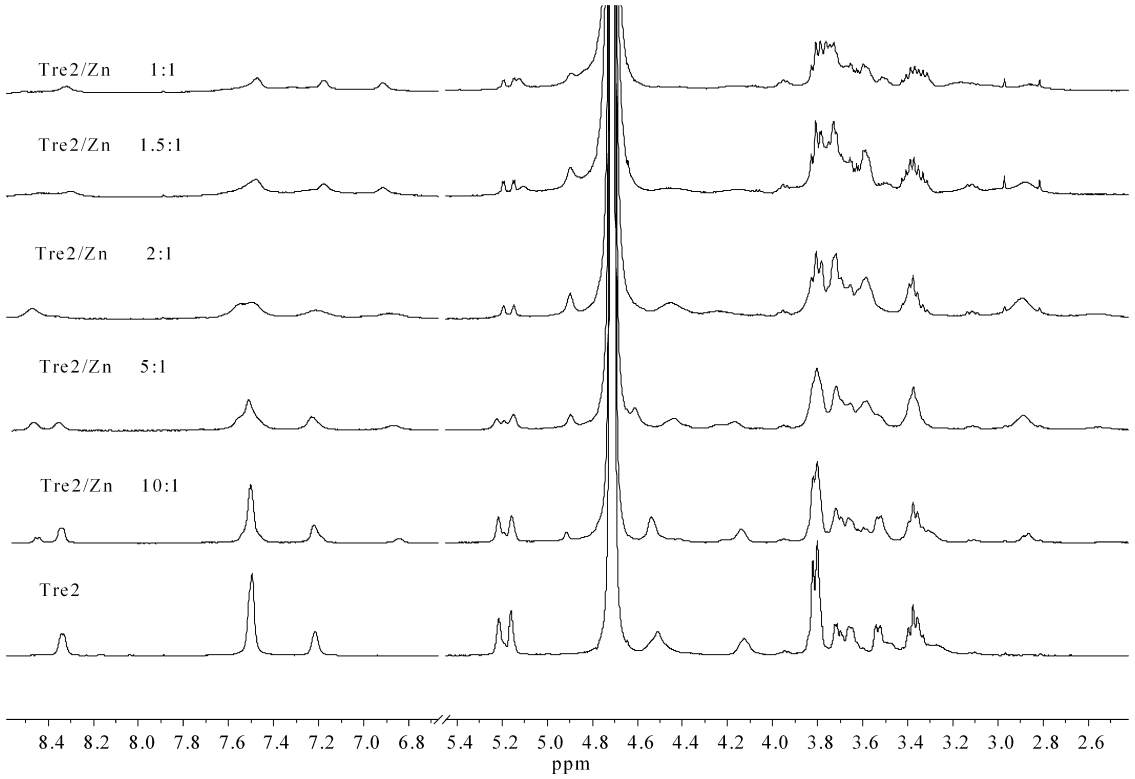

Figure 5. ^{1}H NMR titration of Tre**2** with $ZnCl_2$ in D_2O at pD 7.4.

NMR Spectroscopy. The diamagnetic Zn^{2+} complexes of Tre**1** and Tre**2** were studied by ^{1}H NMR to examine the binding mode.

On the addition of 0.1 and 0.25 equiv of Zn^{2+} to a Tre**1** solution, most protons were slightly shifted and broadened (Figure 4). However, the addition of 0.5 equiv of Zn^{2+} showed significant changes in ^{1}H NMR spectrum of Tre**1**. H-4, H-3, and H-6 protons of the quinoline rings are shifted downfield, and simultaneously H-5 and H-7 upfield. In addition, Tre proton resonances are also affected by the formation of the complex. In particular, H-1A and H-1B are shifted upfield at 5.00 and 4.93 ppm. Overall, the protons of the A ring are more significantly shifted upfield and H-5A, Hs-6A, and H-4A resonate at 3.83, 3.66, 3.48, and 3.19 ppm, respectively. When 1 equiv of Zn^{2+} was added, only slight shifts were observed. This behavior suggests the involvement of the same types of donor atoms in the coordination of Zn^{2+} in both the ML and ML_2 species.

Conversely, as for Tre**2**, a slow ligand exchange process was found with respect to the NMR time scale as the signals of the zinc complex and the free ligand can be individually observed (Figure 5). ^{1}H NMR spectra were carried out at pD = 7.4 in D_2O. The stepwise addition of a $ZnCl_2$ solution led to the appearance of a new set of signals due to the complex species formation. As for the complex species, the H-4 signal of the aromatic moiety shows a downfield shift while the H-5 proton is shifted upfield. Furthermore, new signals due to complex species are present in the aliphatic region. In particular, at $Zn^{2+}/L = 0.2$, Hs-1 of the complex species can be observed at 5.14 and 4.85 ppm. Furthermore, H-1A, H-5A, and H-6A of the complex species are strongly influenced by the metal binding and resonate at 4.85, 4.18, and 2.82 ppm. Moreover, the benzylic protons of the complex species appear at 4.56 and 4.38 ppm.

When zinc is added at M/L = 1, new signals due to a new complex species appear and it seems to be the predominant one in these experimental conditions.

The formation of the ML_2 and ML species can be proposed as well as the involvement of the amino group in the complexation of Zn^{2+} since the aliphatic proton resonances that are mainly influenced by complexation are those of the benzylic CH_2, H-5A and H-6A protons.

Overall, the collected data suggest the formation of the species ML and ML_2 for all the new glycoconjugates. In the case of CuL, the coordination through N (Py), O (phenolate), and an exocyclic nitrogen atom can be invoked. As for ZnL, the involvement of N (Py) and O (phenolate) can be suggested in the metal binding of Tre**1**, whereas the exocyclic N atom is also bound to the metal in the case of Tre**2**.

Unlike ML, a similar behavior in the formation of ML_2 species was observed for Tre**1** (or Glc**1**) and Tre**2** (or Glc**2**), and a coordination environment similar to that of OHQ can be hypothesized.

Antiproliferative Activity. The antiproliferative activity of the new glycoconjugates was tested on three different cell lines (A2780, A549, and SHSY5Y). The effect of the Cu^{2+} ion on their antiproliferative activity was also investigated. In all tested cell lines, the compounds showed IC_{50}s > 100 μM and the presence of copper ions did not influence their cytotoxicity. These results highlight that, under the *in vitro* conditions tested, these derivatives and their copper complexes are not cytotoxic.

Overall, the Tre and Glc derivatives are devoid of significant antiproliferative activity (30 μM is the arbitrary limit to define a significant pharmacological antiproliferative activity). It is worth noting that these new glycoconjugates did not possess antiproliferative activity against SHSY5Y neuroblastoma cells. These cells share the same embryonal origin from the neural crest of the peripheral nerves and ganglia of the sympathetic

DOI: 10.1021/ic502713f
Inorg. Chem. 2015, 54, 2591−2602

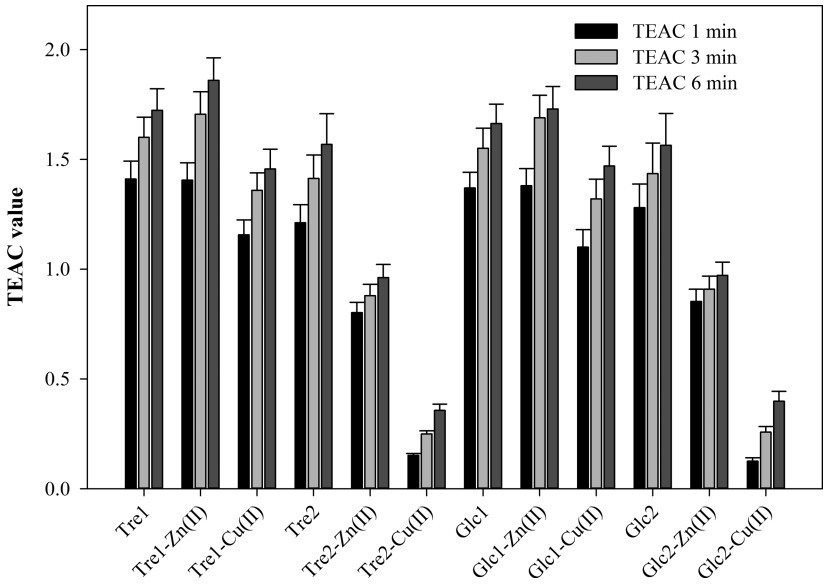

Figure 6. TEAC values at 1, 3, and 6 min for the derivatives. Error bars represent the standard deviation.

nervous system and thus represent a preliminary model for the evaluation of the toxic effect of the compounds on the nervous system.

The new derivatives differ from OHQs or their glucoconjugated prodrugs which were cytotoxic against human cancer cells (IC_{50} values ranging from 0.3 to 8.7 μM) in the same experimental conditions alone and in the presence of Cu^{2+} ion.[14,15]

Antioxidant/Antiradical Activity. Evidence of oxidative stress is widespread in neurodegenerative diseases,[43,44] and in this respect, much effort has been undertaken to target it, developing new and powerful antioxidants.

The antioxidant activity is related to the ability of protecting a biological system against the potentially harmful effect of processes that cause excessive oxidation, involving reactive oxygen nitrogen species (RONS). Several methods are used to measure this activity, and the most commonly used for their ease, speed, and sensitivity are those involving a radical chromogen compound, such as $ABTS^{\bullet+}$ and $DPPH^{\bullet}$ radicals, in order to simulate RONS.

We thus studied the antioxidant activity of these new derivatives via the Trolox Equivalent Antioxidant Capacity (TEAC) assay that determines the quenching rate of 2,2′-azinobis(3-ethylbenzothiazoline-6-sulfonic acid) radical cation ($ABTS^{\bullet+}$) in the presence of antioxidant compounds by means of UV−vis spectroscopy. The ability of the compounds to quench the $ABTS^{\bullet+}$ radical cation was compared to Trolox, a water-soluble analogue of vitamin E. The results, expressed as TEAC values, indicated the high ability of the tested compounds to scavenge the free radical $ABTS^{\bullet+}$ after 1, 3, and 6 min (Figure 6). All compounds are more active than Trolox and CQ, whose activity was previously reported by us.[12] The higher activity compared to that of Trolox is generally associated with a good protective function against oxidative stress.

Free radical scavenging capacity of the trehalose and glucose conjugates could be attributed to the high reactivities of the hydroxyl substituent on the aromatic rings. The nature of substituents (electron-withdrawing, electron donator, inductive effects) has an influence on the H-donating ability of the hydroxyl group.

Tre**1** and Tre**2** exhibit TEAC values that are statistically equivalent to Glc**1** and Glc**2**, respectively. However, their scavenging ability is higher than that of CQ. Probably, the inductive effect of the halogen substituents in CQ destabilizes the phenoxyl radical, reducing its antioxidant ability. On the other hand, the conjugation of OHQ with Tre and Glc increased the stability of the phenoxyl radical, as demonstrated by higher TEAC values compared to CQ.

Continuous absorbance monitoring (within 6 min) shows that these antioxidants differ from Trolox, whose reaction with $ABTS^{\bullet+}$ is complete within the mixing time. Conversely, the TEAC values of glycoconjugates increase within 6 min, suggesting a different kinetics compared to Trolox.

The TEAC assay was also carried out in the presence of an equimolar amount of Zn^{2+} and Cu^{2+}. The presence of Zn^{2+} and Cu^{2+} influences the radical quenching ability of the compounds, in particular for Tre**2** and Glc**2**. These activities can be ascribed to the metal complex species on the basis of the complex stability constants.

The antioxidant activity of the ligands was also determined using $DPPH^{\bullet}$ free radical scavenging assay (Table 3). The time required to reach the steady state in the reaction with $DPPH^{\bullet}$ depends on the nature of the antioxidants. In general, antioxidants can be classified under the categories of fast (<30 min), medium (30 min to 1 h), and slow (>1 h).[45] The reaction time for the glycoconjugates was found to be around 2 h, and thereof, they can be considered as good examples for slow kinetics.

Table 3. Concentration of Tre1, Tre2, Glc1, and Glc2 Needed To Decrease the Initial $DPPH^{\bullet}$ Concentration "EC_{50}" by 50% at 1 h and at the Steady State

compounds	EC_{50} (1 h)	EC_{50} (steady state)
Tre**1**	79 ± 5 μM	55 ± 3 μM
Tre**2**	87 ± 7 μM	61 ± 6 μM
Glc**1**	81 ± 4 μM	59 ± 6 μM
Glc**2**	83 ± 8 μM	57 ± 5 μM

DOI: 10.1021/ic502713f
Inorg. Chem. 2015, 54, 2591−2602

Inhibition of Metal-Induced Amyloid Aggregation. *Zinc-Induced BLG Aggregation.* The aggregation assay of the protein BLG was carried out in order to verify if the new glycoconjugates could inhibit metal-induced protein aggregation. BLG was selected because its heat-induced aggregation could be used as a general model for fibril formation, as previously reported by us.[12]

BLG denaturation and aggregation is strongly influenced by different parameters such as ionic strength, pH, buffer, as well as by transition metal ions, i.e., zinc.

The ability of the derivatives to influence the metal-induced aggregation of BLG was investigated by dynamic light scattering (DLS), and the scattered intensities are reported in Figure 7. A rapid increase of the count rate as a function of the

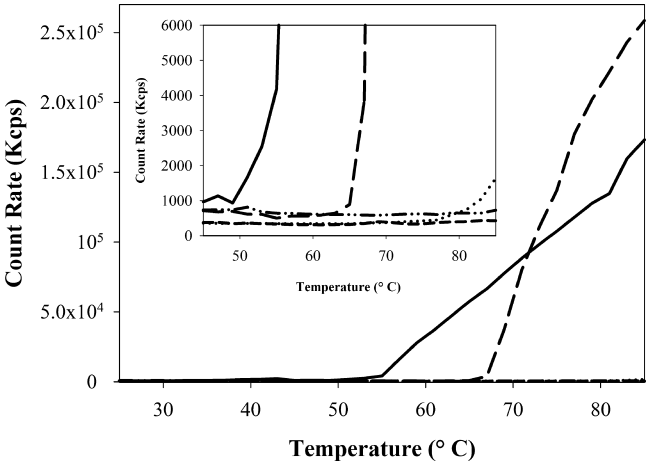

Figure 7. Scattered intensity as a function of temperature for Zn-BLG (—), Zn-Tre**1**-BLG (····), Zn-Tre**2**-BLG (- - -), Zn-Glc**1**-BLG (— — —), and Zn-Glc**2**-BLG (—··—··—).

temperature in the DLS assay is evident in the presence of Zn^{2+} at pH 7.0 (MOPS,10 mM), indicating an aggregation process that starts at about 45−50 °C.

Temperature scanning was also carried out in the presence of the glycoconjugates. In particular, Tre**1** and Tre**2** strongly inhibit the Zn^{2+}-induced thermal aggregation. Furthermore, Tre**2** is more effective in inhibiting the metal-induced aggregation. In fact, a slight increase of the total scattered intensity vs the temperature is observed in the presence of Tre**1**, whereas the total scattered intensity remains essentially unchanged in the case of Tre**2**. Tre is not able to inhibit metal-induced BLG aggregation (data not shown), suggesting the crucial role of the metal binding site in these molecules.

To better examine the role of metal chelation and the sugar on the reduced aggregation, we carried out the temperature scanning DLS assay in the presence of Glc**1** and Glc**2**. It is noteworthy that Glc**1** has a different effect compared to the analogous Tre**1**; the protein aggregation starts at higher temperature (65 °C), indicating that the glucoconjugate delays but not reduces the extent of the Zn^{2+}-induced amyloid formation. This result supports the hypothesis that trehalose could have a role in the stabilization of the protein structure in the experimental conditions, considering that a similar chelating ability can be supposed for Tre**1** and Glc**1** that possess the same donor atom set. The Tre unit could have a synergistic effect in reducing metal-triggered amyloid formation.

Metal-Induced $A\beta_{1\text{-}40}$ and $A\beta_{1\text{-}42}$ Aggregation. The effect of OHQ glycoconjugates on preventing the Cu^{2+}- and Zn^{2+}-induced $A\beta_{1\text{-}40}$ and $A\beta_{1\text{-}42}$ aggregation was assayed.

As shown in Figure 8, the turbidity of the $A\beta_{1\text{-}40}$ solution alone (Ctrl-Cu sample) incubated at 37 °C for 3 h is very small

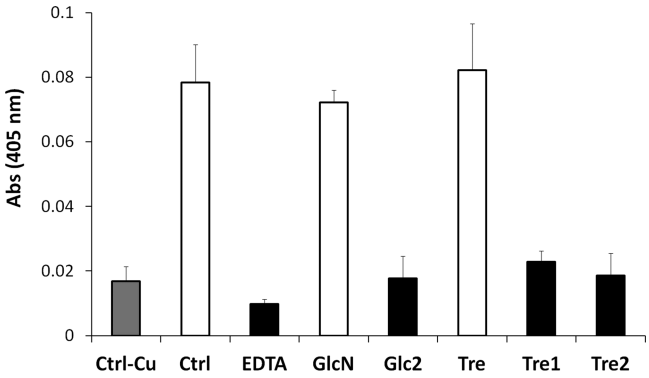

Figure 8. Turbidimetric measurements of $A\beta_{1\text{-}40}$ (20 μM) alone (Ctrl-Cu), with Cu^{2+} (Ctrl) and pre-incubated with EDTA, the OHQ derivatives (Glc**2**, Tre**1** and Tre**2**) or their glycoside moieties (GlcN and Tre).

(0.017 units). As expected, the light scattering of the $A\beta$ peptide solution considerably increases (0.071 units) in the presence of Cu^{2+}, thus confirming the well-known effect of Cu^{2+} ion on speeding up the aggregation of $A\beta_{1\text{-}40}$. This absorbance change is markedly reduced when a well-known metal chelator (EDTA) is co-incubated with $A\beta_{1\text{-}40}$ before the metal ion is added.

Glc**2**, Tre**1**, and Tre**2**, the most active compounds in the BLG aggregation assay, were also able to prevent amyloid aggregation. In fact, the turbidity of the corresponding solutions is not significantly different from that relative to $A\beta_{1\text{-}40}$ alone. This action as inhibitors of Cu^{2+}-induced amyloid aggregation may be reasonably ascribed to Cu^{2+} chelating ability of the OHQ derivatives. This statement is also supported by the lack of any effect on the amyloid aggregation shown by the glycoside moieties (GlcN and Tre). Moreover, the turbidimetric assay revealed that both Cu^{2+} and Zn^{2+} complexes with OHQ are insoluble in the experimental conditions used (data not shown).

The behavior as antiaggregant agents did not basically change when zinc was used (Figure 9). The addition of Zn^{2+} in a solution of $A\beta_{1\text{-}40}$ generates a variation of 0.064 units in absorbance with respect to the $A\beta$ solution. Glc**2**, Tre**1**, and Tre**2**, but not Glc and Tre, significantly reduce such an effect when incubated with $A\beta_{1\text{-}40}$. Hence, the OHQ glycoconjugates act as metal chelators in order to prevent the Zn^{2+}-mediated aggregation of $A\beta_{1\text{-}40}$ and the capacity in inhibiting the amyloid aggregation is related to their ability to complex zinc, as also observed in the BLG assay. Moreover, the Tre derivatives seem to exert their inhibiting action slightly better than the glucose-OHQ conjugate.

Therefore, the glycoconjugation represents a valid strategy to allow the quinoline moiety to exert its metal-binding capability in aqueous solution.

The encouraging results obtained for the metal-induced $A\beta_{1\text{-}40}$ aggregation in the presence of the glycoconjugates led us to carry out the same experiments using $A\beta_{1\text{-}42}$. The last is more toxic than $A\beta_{1\text{-}40}$ because it is more prone to form highly toxic soluble oligomers. Both in the case of Cu^{2+} and Zn^{2+}, the

DOI: 10.1021/ic502713f
Inorg. Chem. 2015, 54, 2591−2602

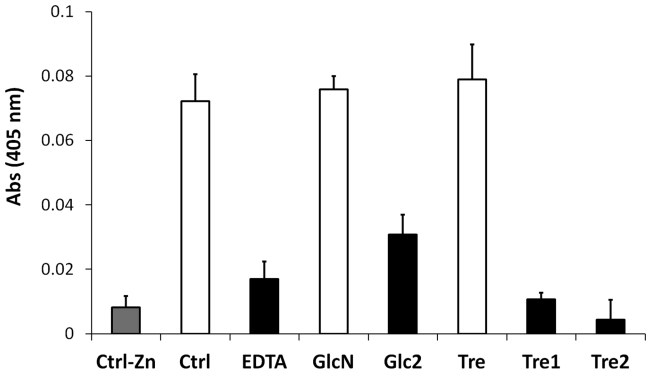

Figure 9. Turbidimetric measurements of A$\beta_{1\text{-}40}$ (20 μM) alone (Ctrl-Zn), with Zn^{2+} (Ctrl) and pre-incubated with EDTA, the OHQ derivatives (Glc**2**, Tre**1**, and Tre**2**) or their glycoside moieties (GlcN and Tre).

findings are very similar to those reported for A$\beta_{1\text{-}40}$ aggregation (Figures S28–S29, Supporting Information): (i) the incubation of metal ions clearly accelerates the aggregation process; (ii) GlcN and Tre show low or negligible effects on the metal-mediated aggregation; (iii) all the HQ-derivatives undoubtedly prevent amyloid aggregation, as well as EDTA.

In order to corroborate the antiaggregant activity of the quinoline derivatives on the aggregation of A$\beta_{1\text{-}42}$ mediated by Cu^{2+} and Zn^{2+} and also to have information about the amyloid species involved in this process, the reactions were also monitored by Native-PAGE/Western blot analysis.

After 3 h incubation at 37 °C, A$\beta_{1\text{-}42}$ is mainly present in solution as monomer and dimer species (lane 1, Figure 10).

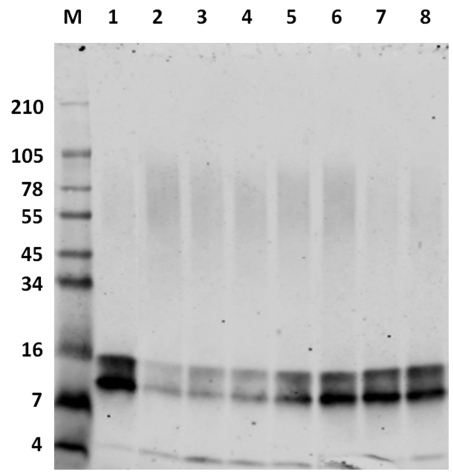

Figure 10. Native PAGE/Western blot analysis of A$\beta_{1\text{-}42}$ alone (1), with Zn^{2+} (2) and pre-incubated with EDTA (5), Tre**1** (6), Tre**2** (7), and Glc**2** (8) or their glycoside moieties Tre (3) and GlcN (4). M is for the marker.

When A$\beta_{1\text{-}42}$ is incubated with Zn^{2+}, the aggregation is speeded up and the amount of the low-molecular-weight (LMW) species decreases (lane 2, Figure 10). The same effect is observed when Tre and GlcN are incubated with the amyloid peptide before the addition of Zn^{2+} (lanes 3 and 4, Figure 10). Conversely, EDTA, Tre**1**, Tre**2**, and Glc**2** quench the effect of Zn^{2+} (lanes 5–8, Figure 10) and the amount of LMW species is similar to that estimated for the incubation of A$\beta_{1\text{-}42}$ alone. These results, along with those of the turbidimetric assay are referred to the early stages of the amyloid aggregation process. Longer incubation periods could reasonably lead to an increase of larger amyloid aggregates, as previously reported,[46,47] but it should not influence the antiaggregant activity of the new OHQ glycoconjugates.

The analysis of the analogous reaction samples in the presence of Cu^{2+} by Native-PAGE/Western blot gave similar results to those obtained with Zn^{2+} (Figure S30, Supporting Information), thus confirming the crucial role that these quinoline derivatives have in reducing the metal-induced aggregation of A$\beta_{1\text{-}42}$.

CONCLUSIONS

Four new chelating glycoconjugates were synthesized and characterized as well as their Zn^{2+} and Cu^{2+} complexes.

One of the most important advantages of these sugar derivatives resides in their good solubility in water that allows for the study of their metal complexes in physiological-like conditions. In particular, the conjugation with Tre is more effective than that with Glc in rendering the OHQ moiety soluble.

Tre**2** can complex Cu^{2+} and Zn^{2+} ions with stability constants higher than those of OHQ involving another donor atom in the metal binding.

Moreover, all compounds are potent antioxidants, as demonstrated by TEAC and DPPH assays, and their antioxidant activity remains significant upon the zinc and copper complexation.

Tre derivatives are also able to strongly inhibit metal-induced protein aggregation and the formation of amyloid fibrils. Glc derivatives exhibit a different behavior compared to Tre conjugates, suggesting a crucial role for trehalose. Therefore, the antiaggregant ability of chelators does not only depend on the binding affinity of the ligands with metals as these derivatives could have other synergistic effects to modulate metal-triggered amyloid formation.

Finally, it is worth pointing out that trehalose derivatives have never been investigated in comparison with their glucose analogues to the best of our knowledge, and therefore, this work provides new insights on the role of sugar in conferring specific properties.

Unlike other OHQ derivatives,[15] the sugar moiety renders these systems nontoxic, as demonstrated by the *in vitro* assay on human cell lines, and could confer better bioavailability. Overall, these glycoconjugates could be potentially suited to the modulation and/or suppression of the oxidative stress and abnormal metal–protein interactions, identified as responsible for the observed toxicity in several neurodegenerative disorders.

ASSOCIATED CONTENT

Supporting Information

Synthetic schemes, NMR (COSY, TOCSY, HSQC), ESI-MS, UV–vis, and CD spectra of the glycoconjugates. This material is available free of charge via the Internet at http://pubs.acs.org.

AUTHOR INFORMATION

Corresponding Author

*E-mail: gr.vecchio@unict.it (G.V.).

Notes

The authors declare no competing financial interest.

DOI: 10.1021/ic502713f
Inorg. Chem. 2015, 54, 2591–2602

■ ACKNOWLEDGMENTS

We thank MIUR (FIRB RINAME, PON01_1078, FIRB_MERIT_RBN-E08HWLZ) for financial support.

■ REFERENCES

(1) Cavalli, A.; Bolognesi, M. L.; Minarini, A.; Rosini, M.; Tumiatti, V.; Recanatini, M.; Melchiorre, C. *J. Med. Chem.* **2008**, *51*, 347−372.
(2) Viles, J. H. *Coord. Chem. Rev.* **2012**, *256*, 2271−2284.
(3) Kozlowski, H.; Luczkowski, M.; Remelli, M.; Valensin, D. *Coord. Chem. Rev.* **2012**, *256*, 2129−2141.
(4) Rodríguez-Rodríguez, C.; Telpoukhovskaia, M.; Orvig, C. *Coord. Chem. Rev.* **2012**, *256*, 2308−2332.
(5) Sampson, E.; Jenagaratnam, L.; McShane, R. *Cochrane Database Syst. Rev.* **2008**, *1*, CD005380.
(6) Cahoon, L. *Nat. Med.* **2009**, *15*, 356−359.
(7) Bush, A. I.; Tanzi, R. E. *Neurotherapeutics* **2008**, *5*, 421−432.
(8) http://pranabio.com/news/.
(9) Nguyen, M.; Robert, A.; Sournia-Saquet, A.; Vendier, L.; Meunier, B. *Chem.—Eur. J.* **2014**, *20*, 6771−6785.
(10) Ceccom, J.; Coslédan, F.; Halley, H.; Francès, B.; Lassalle, J. M.; Meunier, B. *PLoS One* **2012**, *7*, e43105.
(11) Oliveri, V.; Puglisi, A.; Viale, M.; Aiello, C.; Sgarlata, C.; Vecchio, G.; Clarke, J.; Milton, J.; Spencer, J. *Chem.—Eur. J.* **2013**, *19*, 13946−13955.
(12) Oliveri, V.; Attanasio, F.; Puglisi, A.; Spencer, J.; Sgarlata, C.; Vecchio, G. *Chem.—Eur. J.* **2014**, *20*, 8954−8964.
(13) Oliveri, V.; Bellia, F.; Vecchio, G. *ChemPlusChem* **2015**, DOI: 10.1002/cplu.201402450.
(14) Oliveri, V.; Giuffrida, M. L.; Vecchio, G.; Aiello, C.; Viale, M. *Dalton Trans.* **2012**, *41*, 4530−4535.
(15) Oliveri, V.; Viale, M.; Caron, G.; Aiello, C.; Gangemi, R.; Vecchio, G. *Dalton Trans.* **2013**, *42*, 2023−2034.
(16) Oliveri, V.; Viale, M.; Aiello, C.; Vecchio, G. *J. Inorg. Biochem.* **2015**, *142*, 101−108.
(17) Elbein, A. D.; Pan, Y. T.; Pastuszak, I.; Carroll, D. *Glycobiology* **2003**, *13*, 17R−27R.
(18) Subrata, P.; Sandip, P. *J. Phys. Chem. B* **2015**, *119*, 1598−1610.
(19) Tonnis, W. F.; Mensink, M. A.; de Jager, A.; van der Voort Maarschalk, K.; Frijlink, H. W.; Hinrichs, W. L. J. *Mol. Pharmaceutics* **2015**, DOI: 10.1021/mp500423z.
(20) Singer, M. A.; Lindquist, S. *Mol. Cell* **1998**, *1*, 639−648.
(21) Liu, R.; Barkhordarian, H.; Emadi, S.; Park, C. B.; Sierks, M. R. *Neurobiol. Dis.* **2005**, *20*, 74−81.
(22) Tanaka, M.; Machida, Y.; Niu, S.; Ikeda, T.; Jana, N. R.; Doi, H.; Kurosawa, M.; Nekooki, M.; Nukina, N. *Nat. Med.* **2004**, *10*, 148−154.
(23) Yu, W. B.; Jiang, T.; Lan, D. M.; Lu, J. H.; Yue, Z. Y.; Wang, J.; Zhou, P. *Arch. Biochem. Biophys.* **2012**, *523*, 144−150.
(24) Béranger, F.; Crozet, C.; Goldsborough, A.; Lehmann, S. *Biochem. Biophys. Res. Commun.* **2008**, *374*, 44−48.
(25) Jiang, T.; Yu, W. B.; Yao, T.; Zhi, X. L.; Pan, L. F.; Wang, J.; Zhou, P. *RSC Adv.* **2013**, *3*, 9500−9508.
(26) Grasso, G. I.; Arena, G.; Bellia, F.; Maccarrone, G.; Parrinello, M.; Pietropaolo, A.; Vecchio, G.; Rizzarelli, E. *Chem.—Eur. J.* **2011**, *17*, 9448−9455.
(27) Grasso, G. I.; Arena, G.; Bellia, F.; Rizzarelli, E.; Vecchio, G. *J. Inorg. Biochem.* **2014**, *131*, 56−63.
(28) Im, J.; Kim, S.; Jeong, Y.-H.; Kim, W.; Lee, D.; Lee, W. S.; Chang, Y.-T.; Kim, K.-T.; Chung, S.-K. *Med. Chem. Commun.* **2013**, *4*, 310−316.
(29) Grasso, G. I.; Gentile, S.; Giuffrida, M. L.; Satriano, C.; Sgarlata, C.; Sgarzi, M.; Tomaselli, G.; Arena, G.; Prodi, L. *RSC Adv.* **2013**, *3*, 24288−24297.
(30) Flaschka, H. A. *EDTA Titrations*; Pergamon: New York, 1959.
(31) Bonomo, R. P.; Calì, R.; Cucinotta, V.; Impellizzeri, G.; Rizzarelli, E. *Inorg. Chem.* **1986**, *25*, 1641−1646.
(32) Arena, G.; Rizzarelli, E.; Sammartano, S.; Rigano, C. *Talanta* **1979**, *26*, 1−14.
(33) Gans, P.; Sabatini, A.; Vacca, A. *Talanta* **1996**, *43*, 1739−1753.
(34) Alderighi, L.; Gans, P.; Ienco, A.; Peters, D.; Sabatini, A.; Vacca, A. *Coord. Chem. Rev.* **1999**, *184*, 311−318.
(35) Ha, C.; Ryu, J.; Park, C. B. *Biochemistry* **2007**, *46*, 6118−6125.
(36) Atwood, C. S.; Moir, R. D.; Huang, X.; Scarpa, R. C.; Bacarra, N. M.; Romano, D. M.; Hartshorn, M. A.; Tanzi, R. E.; Bush, A. I. *J. Biol. Chem.* **1998**, *273*, 12817−12826.
(37) Smith, R. M.; Martell, A. E. *Critical Stability Constants: Amines*; Springer: Boston, MA, 1975; Vol. *2*, p 223.
(38) Budimir, A.; Humbert, N.; Elhabiri, M.; Osinska, I.; Biruš, M.; Albrecht-Gary, A.-M. *J. Inorg. Biochem.* **2011**, *105*, 490−496.
(39) Jones, J. G.; Poole, J. B.; Tomkinson, J. C.; Williams, R. J. P. *J. Chem. Soc.* **1958**, 2001−2009.
(40) Kenche, V. B.; Zawisza, I.; Masters, C. L.; Bal, W.; Barnham, K. J.; Drew, S. C. *Inorg. Chem.* **2013**, *52*, 4303−4318.
(41) Farruggia, G.; Iotti, S.; Prodi, L.; Montalti, M.; Zaccheroni, N.; Savage, P. B.; Trapani, V.; Sale, P.; Wolf, F. I. *J. Am. Chem. Soc.* **2006**, *128*, 344−350.
(42) Stevenson, R. L.; Freiser, H. *Anal. Chem.* **1967**, *39*, 1354−1358.
(43) Radi, E.; Formichi, P.; Battisti, C.; Federico, A. *J. Alzheimer's Dis.* **2014**, *42*, S125−S152.
(44) Melo, A.; Monteiro, L.; Lima, R. M.; de Oliveira, D. M.; de Cerqueira, M. D.; El-Bachá, R. S. *Oxid. Med. Cell. Longevity* **2011**, *2011*, 467180.
(45) Mishra, K.; Ojha, H.; Chaudhury, N. K. *Food Chem.* **2012**, *130*, 1036−1043.
(46) Sharma, A. K.; Pavlova, S. T.; Kim, J.; Finkelstein, D.; Hawco, N. J.; Rath, N. P.; Kim, J.; Mirica, L. M. *J. Am. Chem. Soc.* **2012**, *134*, 6625−6636.
(47) Choi, J.-S.; Braymer, J. J.; Nanga, R. P. R.; Ramamoorthy, A.; Lim, M. H. *Proc. Natl. Acad. Sci. U.S.A.* **2010**, *107*, 21990−21995.

DOI: 10.1021/ic502713f
Inorg. Chem. 2015, 54, 2591−2602